



HAL
open science

Retrieval of the spectral diffuse attenuation coefficient $K_d(\lambda)$ in open and coastal ocean waters using a neural network inversion,

Cédric Jamet, Hubert Loisel, D. Dessailly

► **To cite this version:**

Cédric Jamet, Hubert Loisel, D. Dessailly. Retrieval of the spectral diffuse attenuation coefficient $K_d(\lambda)$ in open and coastal ocean waters using a neural network inversion,. *Journal of Geophysical Research*, 2012, 117, pp.C10. 10.1029/2012JC008076 . hal-00823342

HAL Id: hal-00823342

<https://hal.science/hal-00823342>

Submitted on 22 Jun 2021

HAL is a multi-disciplinary open access archive for the deposit and dissemination of scientific research documents, whether they are published or not. The documents may come from teaching and research institutions in France or abroad, or from public or private research centers.

L'archive ouverte pluridisciplinaire **HAL**, est destinée au dépôt et à la diffusion de documents scientifiques de niveau recherche, publiés ou non, émanant des établissements d'enseignement et de recherche français ou étrangers, des laboratoires publics ou privés.

Copyright

Retrieval of the spectral diffuse attenuation coefficient $K_d(\lambda)$ in open and coastal ocean waters using a neural network inversion

C. Jamet,¹ H. Loisel,¹ and D. Dessailly¹

Received 31 March 2012; revised 11 September 2012; accepted 13 September 2012; published 27 October 2012.

[1] The diffuse attenuation coefficient, $K_d(\lambda)$ is a fundamental radiometric parameter that is used to assess the light availability in the water column. A neural network approach is developed to assess $K_d(\lambda)$ at any visible wavelengths from the remote sensing reflectances as measured by the SeaWiFS satellite sensor. The neural network (NN) inversion is trained using a combination of simulated and in-situ data sets covering a broad range of $K_d(\lambda)$, between 0.0073 m^{-1} at 412 nm and 12.41 m^{-1} at 510 nm. The performance of the retrieval is evaluated against two data sets, one consisting of mainly synthetic data while the other one contains in-situ data only and is compared to those obtained with previous published empirical (NASA, Morel and Maritorena (2001) and Zhang and Fell (2007)) and semi-analytical (Lee et al., 2005b) algorithms. On the in-situ data set from the COASTLOOC campaign, the retrieval accuracy of the present algorithm is quite similar to published algorithms for oligotrophic and mesotrophic ocean waters. But for $K_d(490) > 0.25 \text{ m}^{-1}$, the NN approach allows to retrieve $K_d(490)$ with a much better accuracy than the four other methods. The results are consistent when compared with other SeaWiFS wavelengths. This new inversion is as suitable in the open ocean waters as in the turbid waters. The work here is straightforwardly applicable to the MERIS sensor and with few changes to the MODIS-AQUA sensor. The algorithm in matlab and C code is provided as auxiliary material.

Citation: Jamet, C., H. Loisel, and D. Dessailly (2012), Retrieval of the spectral diffuse attenuation coefficient $K_d(\lambda)$ in open and coastal ocean waters using a neural network inversion, *J. Geophys. Res.*, 117, C10023, doi:10.1029/2012JC008076.

1. Introduction

[2] The diffuse attenuation coefficient for downwelling irradiance, $K_d(\lambda)$ (in m^{-1}), where λ is the wavelength of light, is a water property related to light penetration and availability in aquatic ecosystems. Light availability plays a critical role in the regulation of physical and biogeochemical processes in the upper ocean, such as the heat transfer in the upper layer of the ocean [Lewis et al., 1990; Morel and Antoine, 1994; Sathyendranath et al., 1989], phytoplankton photosynthesis in the ocean euphotic zone [Platt et al., 1988; Sathyendranath et al., 1991], and in-water visibility [Preisendorfer, 1986; Tyler, 1968]. $K_d(\lambda)$ is an apparent optical property (AOP) whose variability is governed by changes in the inherent optical properties (IOP) of the water body and sea surface irradiance conditions [Kirk, 1984, 1991; Morel and Loisel, 1998; Preisendorfer, 1975]. The latter depend on the sun zenith angle θ_s , diffuse sky

irradiance, and sea surface state (wind speed). Accurate determination of $K_d(\lambda)$ is critical to being able to analyze and understand those processes.

[3] Satellite observation is the only effective method to provide large-scale maps of $K_d(\lambda)$ over basin and global scales at high spatial and temporal resolutions. The ocean color remote sensing of the diffuse attenuation coefficient corresponds to the average irradiance attenuation coefficient within the upper layer, delimited by the first attenuation depth at which the downwelling irradiance is reduced to 37% of its surface value. The assessment of the diffuse attenuation coefficient from ocean color algorithms is essentially performed at 490 nm. Empirical methods estimate $K_d(490)$ either directly from the blue-to-green [Austin and Petzold, 1981; Mueller, 2000; Werdell and Bailey, 2005] or blue-to-red ratios [Doron et al., 2007; Kratzer et al., 2008; Wang et al., 2009; Zhang and Fell, 2007]. But these latter methods only estimate K_d at 490 nm. Based on $K_d(490)$, $K_d(\lambda)$ can be estimated for other wavelengths (λ) by using empirical relationships between $K_d(490)$ and $K_d(\lambda)$ [Austin and Petzold, 1986; Kishino et al., 1996]. Empirical algorithms based on spectral relationships between $K_d(\lambda)$ and the chlorophyll-a concentration, $Chla$, allow, by construction, the retrieval of $K_d(\lambda)$ at any visible wavelengths [Morel, 1988; Morel and Maritorena, 2001; Morel et al., 2007]. However, these published formulations

¹LOG/ULCO/CNRS, Wimereux, France.

Corresponding author: C. Jamet, Laboratoire d'Océanologie et de Géosciences, UMR 8187, CNRS, Université du Littoral-Côte d'Opale, 32 ave. Foch, FR-62930 Wimereux, France. (cedric.jamet@univ-littoral.fr)

©2012. American Geophysical Union. All Rights Reserved.
0148-0227/12/2012JC008076

strongly depend on field data sets used for their developments, which is problematic for global applications offered by satellite observation of ocean color. Semi-analytical algorithms do not present such limitation, as they are based on semi-analytical relationships between IOP and $K_d(\lambda)$ [Lee et al., 2005b]. In the semi-analytical method, $K_d(490)$ is estimated from the absorption and backscattering coefficients through a semi-analytical model [Lee et al., 2002, 2005b, 2007].

[4] Lee et al. [2005a] showed that empirical methods [Austin and Petzold, 1981; Mueller, 2000; Morel and Maritorena, 2001], produced satisfactory estimates in clear open ocean waters, i.e. for low values of $K_d (<0.25 \text{ m}^{-1})$, but they generally failed to provide accurate estimates in turbid waters (high values of K_d), using data collected in three different regions that cover open ocean and coastal waters (Gulf of Mexico, the Arabian and the Baltic Seas). The semi-analytical method of Lee et al. [2005b] did not show such limitations. In order to avoid the limitations of the empirical algorithms based on blue/green ratios, alternative wavelengths band ratios with higher red wavelengths could be used and have shown improvements for MODIS and MERIS ocean color sensors [Doron et al., 2007; Kratzer et al., 2008; Wang et al., 2009].

[5] Neural networks (NN) are good candidates for modeling inverse functions in geophysical and remote sensing applications [Atkinson and Tatnall, 1997; Badran and Thiria, 2002; Gardner and Dorling, 1998; Krasnopolsky and Schiller, 2003; Krasnopolsky, 2007; Thiria et al., 1993]. An NN, if properly parameterized, can yield retrievals that are accurate and relatively insensitive to reasonable noise levels, because noise is introduced and accounted for during the training process. The type of NN used in this study is the Multi-Layer Perceptron (MLP) [Rumelhart et al., 1986] which can be seen as a generic technique for the nonlinear approximation of nonlinear continuous and almost continuous mappings [Cybenko, 1989; Hornik et al., 1989; Pinkus, 1999]. The MLP is an empirical method that allows the inclusion of more information as inputs than the classic linear or polynomial regressions. A number of studies in ocean color were published using MLP inversion, for the atmospheric correction processing [Brajard et al., 2006a, 2006b, 2008; Jamet et al., 2004, 2005; Schroeder et al., 2007], the estimation of $Chla$ concentration [Buckton et al., 1999; D'Alimonte and Zibordi, 2003; Gonzales Vilas et al., 2011; Gross et al., 2000; Keiner and Brown, 1999; Schiller and Doerffer, 1997; Tanaka et al., 2004; Zhang et al., 2003], or the inherent optical properties retrieval [Bricaud et al., 2007; Doerffer and Schiller, 2007; Ioannou et al., 2011], among others. This study is the first attempt to use this type of statistical inversion for estimating the diffuse attenuation coefficient from ocean color satellite data at the SeaWiFS wavelengths.

[6] In this paper, we briefly describe the empirical and semi-analytical methods previously published for deriving $K_d(490)$ (and $K_d(\lambda)$) from ocean color remote sensing. Then, we present the synthetic and in-situ data sets used for the training of the NN inversion and its validation and comparison to existing algorithms. A brief mathematical concept of the NN is given in section 4. Section 5 presents the validation of the NN inversion and its comparison to four existing algorithms using two types of data sets. One

SeaWiFS image is presented as an example of application of the new NN inversion in the English Channel/North Sea. The work presented in this study focuses on the Sea-viewing Wide Field-of-view Sensor (SeaWiFS) but the method is straightforwardly applicable for the Moderate Resolution Imaging Spectroradiometer (MODIS) or the Medium Resolution Imaging Spectrometer (MERIS) sensors.

2. Existing Algorithms for the Estimation of $K_d(\lambda)$

[7] This section presents four different ocean color algorithms previously developed to compute the diffuse attenuation coefficient at different wavelengths (two only at $\lambda = 490 \text{ nm}$ and the two others at any wavelengths), and which are taken into account in the inter-comparison exercise.

2.1. One-Step Empirical Methods

[8] In the framework of the Coastal Zone Color Scanner (CZCS) mission, Austin and Petzold [1981] proposed an algorithm to derive $K_d(490)$ from the water-leaving radiances, L_w , estimated at $\lambda_1 = 443 \text{ nm}$ and $\lambda_2 = 550 \text{ nm}$ as follows:

$$K_d(490) = K_w(490) + 0.0883 \times \left(\frac{L_w(443)}{L_w(550)} \right)^{-1.491} \quad (1)$$

with $K_w(490)$, the attenuation coefficient for pure sea water ($K_w = 0.022 \text{ m}^{-1}$).

[9] To assess the diffuse attenuation coefficient at 490 nm from the SeaWiFS sensor, Mueller [2000] proposed a variant of the previous equation:

$$K_d(490) = K_w(490) + 0.15645 \times \left(\frac{L_w(490)}{L_w(555)} \right)^{-1.5401} \quad (2)$$

with a K_w value of 0.016 m^{-1} [Mueller, 2000]. This version was modified in 2005 using the remote sensing reflectance R_{rs} instead of the water-leaving radiances L_w , as input parameters (http://oceancolor.gsfc.nasa.gov/REPROCESSING/SeaWiFS/R5.1/k490_update.html) using the following equation:

$$K_d(490) = 0.1853 \left(\frac{R_{rs}(490)}{R_{rs}(555)} \right)^{-1.349} \quad (3)$$

[10] The NASA operational algorithm for deriving $K_d(490)$ (<http://oceancolor.gsfc.nasa.gov/REPROCESSING/R2009/kdv4/>) was updated using in situ data from the NASA bio-Optical Marine Algorithm Data set (NOMAD [Werdell and Bailey, 2005]). The algorithm is described by the polynomial best fit that relates the log-transformed $K_d(490)$ variable to a log-transformed ratio of remote-sensing reflectances. The polynomial form replaces the power-law form employed in previous K_d algorithms (equations (1), (2), and (3)) and uses the remote-sensing reflectances (R_{rs}) instead of the water-leaving radiances L_w or the normalized value, nL_w :

$$K_d(490) = 10^{(0.8515 - 1.8263X + 1.8714X^2 - 2.4414X^3 - 1.0690X^4)} + 0.0166 \quad (4)$$

Table 1. Range and Median Values of $K_d(490)$, $R_{rs}(490)$ and $R_{rs}(555)$ for Each Data Set Used for the Training of the NN Inversion^a

	BOUM	NOMAD	IOCCG	Synthetic-Turbid
N $K_d(490)$ (m^{-1})	60	1308	9000	1656
Range Median $R_{rs}(490)$ (sr^{-1})	[0.008; 0.34] 0.038	[0.019; 2.29] 0.25	[0.017; 2.53] 0.20	[0.056; 7.73] 0.86
Range Median $R_{rs}(555)$ (sr^{-1})	[0.0050; 0.0060] 0.0059	[0.00037; 0.0096] 0.0032	[0.00060; 0.0175] 0.0054	[0.0012; 0.0278] 0.0082
Range Median Reference	[0.0011; 0.00017] 0.0014 <i>Loisel et al. [2011]</i>	[0.00042; 0.0179] 0.0030 <i>Werdell and Bailey [2005]</i>	[0.00089; 0.0297] 0.0046 <i>IOCCG [2006]</i>	[0.018; 0.049] 0.014 section 3.1

^aN represents the total number of points per data set (for all SeaWiFS wavelengths).

with $X = \log_{10} \left(\frac{R_{rs}(490)}{R_{rs}(555)} \right)$. This method will be thereafter referred to as $K_d^{Werdell}$.

[11] As shown by *Mueller [2000]*, the empirical algorithm using a fixed ratio of R_{rs} generally works well in clear waters ($K_d(490) \leq 0.25 m^{-1}$) but shows significant uncertainties for higher values of $K_d(490)$ (i.e., in turbid waters). An alternative approach was proposed by *Zhang and Fell [2007]* to improve the determination of $K_d(490)$ in turbid waters. This method, thereafter referred to as K_d^{Zhang} , uses a switching point to deal with $K_d(490)$ values higher than $0.5 m^{-1}$, as follows:

$$\text{if } \frac{R_{rs}(490)}{R_{rs}(555)} \geq 0.85 \text{ then } K_d(490) = 10^{(-0.843 - 1.459X - 0.101X^2 - 0.811X^3)} \quad (5)$$

with $X = \log_{10} \left(\frac{R_{rs}(490)}{R_{rs}(555)} \right)$ and

$$\text{if } \frac{R_{rs}(490)}{R_{rs}(555)} < 0.85 \text{ then } K_d(490) = 10^{(0.094 - 1.302X + 0.247X^2 - 0.021X^3)} \quad (6)$$

with $X = \log_{10} \left(\frac{R_{rs}(490)}{R_{rs}(670)} \right)$

[12] These two empirical algorithms ($K_d^{Werdell}$ and K_d^{Zhang}) allow to estimate K_d only at $\lambda = 490$ nm.

2.2. Two-Step Empirical Method

[13] Another way to estimate the diffuse attenuation coefficient is to use a two-step method, with *Chla* as an intermediate parameter [*Morel, 1988; Morel and Maritorena, 2001*]. In the present study, *Chla* is derived from the empirical OC4v6 algorithm (<http://oceancolor.gsfc.nasa.gov/REPROCESSING/R2009/ocv6/>) as follows:

$$\text{chl } a = 10^{(a_0 + a_1X + a_2X^2 + a_3X^3 + a_4X^4)} \quad (7)$$

with $X = \log(R_{rs}^1/R_{rs}^2)$ where $R_{rs}^1 = \max(R_{rs}(443), R_{rs}(490), R_{rs}(510))$ and $R_{rs}^2 = R_{rs}(555)$; $a_0 = 0.3272$, $a_1 = -2.9940$, $a_2 = 2.7218$, $a_3 = -1.2259$ and $a_4 = -0.5683$.

[14] Then, the K_d versus *Chla* empirical relationships are used to calculate $K_d(\lambda)$ at any visible wavelengths:

$$K_d(\lambda) = K_w(\lambda) + a_0(\lambda) * (\text{Chla})^{a_1(\lambda)} \quad (8)$$

[15] For $\lambda = 490$ nm, $K_w = 0.0166 m^{-1}$, $a_0 = 0.07242$ and $a_1 = 0.68955$. This method will be thereafter referred to as K_d^{Morel} . This method has been developed using in-situ data in oligotrophic and mesotrophic waters, with relatively low values of $K_d(\lambda)$ ($< 0.5 m^{-1}$). The evaluation of K_d^{Morel} is the

combination of OC4V6 and the relationship between *Chla* and $K_d(\lambda)$.

2.3. A Semi-analytical Approach

[16] The change of the diffuse attenuation coefficient with variations of the IOP and the solar zenith angle has long been studied through radiative transfer calculations [*Gordon, 1989; Kirk, 1984, 1991; Lee et al., 2005b; Morel and Loisel, 1998*]. Based on these modeling studies, semi-analytical relationships have been developed. For instance, through Monte Carlo modeling, *Kirk [1984]* proposed a simple parameterization between $K_d(\lambda)$, the solar zenith angle and the absorption and scattering coefficients. *Morel and Loisel [1998]* improved this parameterization by taking into account the effect of the variations in the shape of the volume scattering function, as well as the sky conditions. In contrast to these studies, *Lee et al. [2002]* parameterized $K_d(\lambda)$ as a function of the absorption and backscattering coefficients, which can be both estimated from satellite ocean color observations. The model can be written as:

$$K_d(\lambda) = (1 + 0.005\theta_s) \times a(\lambda) + 4.18 \times (1 - 0.52 \times \exp(-10.8a(\lambda))) \times b_b(\lambda) \quad (9)$$

where θ_s is the solar zenith angle, and $a(\lambda)$ and $b_b(\lambda)$, the absorption and backscattering coefficients, respectively. These two parameters are retrieved from the remote sensing reflectances, R_{rs} , at wavelengths 443, 490, 555 and 670 nm with the Quasi-Analytical Algorithm (QAA) [*Lee et al., 2002, 2005a, 2007*]. The measured values of θ_s are available in the different data sets used for this study. This method will be thereafter referred to as K_d^{Lee} .

3. Data

3.1. Training Data

[17] The training data set includes R_{rs} and K_d data points that were issued from either field or synthetic data sets, at the SeaWiFS wavelengths. The main characteristics of these four different data sets are summarized in Table 1.

[18] The full data set is mainly composed of the synthetic data set created by the International Ocean Color Coordinating Group (IOCCG) working group on Ocean Color Algorithms [*IOCCG, 2006*] as well as the NOMAD data set [*Werdell and Bailey, 2005*]. When the wavelengths in the IOCCG database differed from that of the SeaWiFS sensor, the remote-sensing reflectances at 410, 440, 490, 510, 550, 560 and 670 nm were interpolated to get R_{rs} at the corresponding SeaWiFS wavelengths using a spline method. In this synthetic data set, the inherent optical properties (IOPs) were generated with various available/reasonable optical/bio-optical parameters/models to account for the

Table 2. Median, Standard Deviation, and Minimum and Maximum Values of $K_d(\lambda)$ of the COASTLOOC Data Set

	$K_d(412)$	$K_d(443)$	$K_d(490)$	$K_d(510)$	$K_d(555)$	$K_d(670)$
Median (m^{-1})	1.05	0.75	0.46	0.41	0.32	0.71
Standard deviation (m^{-1})	1.00	0.80	0.60	0.56	0.44	0.41
Minimum (m^{-1})	0.012	0.029	0.023	0.021	0.019	0.27
Maximum (m^{-1})	4.81	4.02	3.14	2.94	2.46	2.67

natural variability encountered in natural waters. R_{rs} and K_d were generated using the HydroLight software [Mobley, 1994, 1995] with these IOPs and different sun zenith angles as inputs parameters. More details are given in the IOCCG report #5 [IOCCG, 2006].

[19] The NOMAD data set gathered field measurements collected in optically very diverse waters. Only 218 comitant observations (per wavelength) of $R_{rs}(\lambda)$ and $K_d(\lambda)$ were available. The $K_d(490)$ values cover a broad range of trophic waters (from oligotrophic to turbid waters, Table 1).

[20] For completing these two data sets and having a large range of $K_d(\lambda)$ representing ocean waters from very-oligotrophic to very turbid situations, two others data sets were added. The third data set corresponds to field measurements collected in very oligotrophic areas of the Mediterranean Sea during the BOUM experiment in 2008 [Loisel et al., 2011]. In this third data set, $K_d(\lambda)$ vary between 0.008 m^{-1} and 0.34 m^{-1} , with a median value of 0.08 m^{-1} (Table 1), which are very low values for $K_d(\lambda)$. The fourth data set corresponds to very turbid waters (named as synthetic-turbid data set in Table 1) and is developed through radiative transfer computations. The details about this synthetic data set are given in Appendix A.

[21] The number of ($R_{rs}(\lambda)$, $K_d(\lambda)$) pairs is 1500, 218, 10, 120 for the IOCCG, NOMAD, BOUM, synthetic-turbid data sets per wavelength, respectively (Table 1). The range of $K_d(490)$ and median values and associated R_{rs} at 490 and 555 nm for each data set is summarized in Table 1. Most of the $K_d(\lambda)$ values are below 0.5 m^{-1} . For all wavelengths, 4121 $K_d(\lambda)$ out of 10656 and 553 $K_d(\lambda)$ out of 1368 are $<0.25 \text{ m}^{-1}$ in the synthetic and in-situ data sets, respectively. The whole in-situ and synthetic data set (Table 1) has then been divided into two sub-data sets: 80% of the data (sub-data set 1) were randomly selected for the training phase of the neural network (i.e. determination of its parameters, see section 4) while the rest (sub-data set 2) were used to evaluate the capacity of the neural network to retrieve $K_d(\lambda)$ from $R_{rs}(\lambda)$.

3.2. Validation Database

[22] While the sub-data set 2 is also used for the validation and algorithm comparison phases, a fully independent data set was taken for that purpose. The COASTLOOC data set [Babin et al., 2003a] was used to evaluate the neural network approach, and to compare its performance with existing methods. The COASTLOOC data set gathered field measurements performed in 1997 and 1998 in European coastal waters and is comprised of 420 observations per wavelength. It is entirely independent from the in-situ data sets, i.e. no COASTLOOC data were integrated into NOMAD or BOUM. These data cover a large variability in terms of water types with values of $K_d(490)$ ranging from

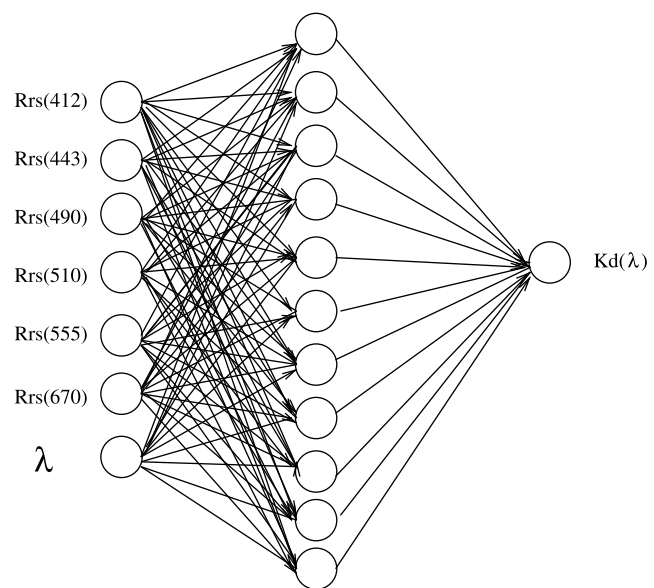
0.023 m^{-1} to 3.14 m^{-1} (Table 2). For our study, this data set has been reduced to 132 data points (per λ), because of the constraints on the spectral values of R_{rs} and $K_d(\lambda)$, as values of R_{rs} at 412, 443, 490, 510, 555 and 670 nm are needed as inputs of the neural network. The median and standard deviation values of $K_d(\lambda)$ are provided in Table 2.

[23] The irradiance reflectance just below the sea surface, $R(0^-)$, was available in the COASTLOOC data set instead of the remote sensing reflectance, R_{rs} . Therefore, prior to any evaluation, $R(0^-)$ needed to be converted into R_{rs} . The formulation used by Zhang and Fell [2007], who also took the COASTLOOC data set for their $K_d(490)$ retrieval evaluation, was adopted: $R_{rs} = 0.133 \times R(0^-)$.

4. Neural Network Inversion

[24] The type of neural network used in this study is the Multi-Layer Perceptron (MLP). A neuron is an elementary transfer function that provides an output s when an input A is applied. An MLP is a set of interconnected neurons (Figure 1). Each neuron receives from and sends signals only to the neurons to which it is connected. Thanks to this association of elementary tasks, an MLP is able to solve complex inverse problems. The specificity of an MLP depends on the topology of the neurons (number of layers, numbers of neurons on each layer) and on the connection weights w_{ij} from neuron j to neuron i . The MLP architecture has one layer with the inputs, one layer broadcasting the outputs, and one or more intermediate layers (the so-called hidden layers). The network used in this study is fully connected (Figure 1).

[25] The w_{ij} weight values were computed through a training phase, using the training data set (i.e., sub-data set 1). We minimized a cost function defined as the quadratic difference between the desired and the computed outputs, the w_{ij} being the control variables. For that purpose, we used a conjugate-gradient technique, that is an iterative optimization method

**Figure 1.** Architecture of the Multi-Layer Perceptron with 7 inputs, one hidden layer of 11 neurons and 1 output, $K_d(\lambda)$.

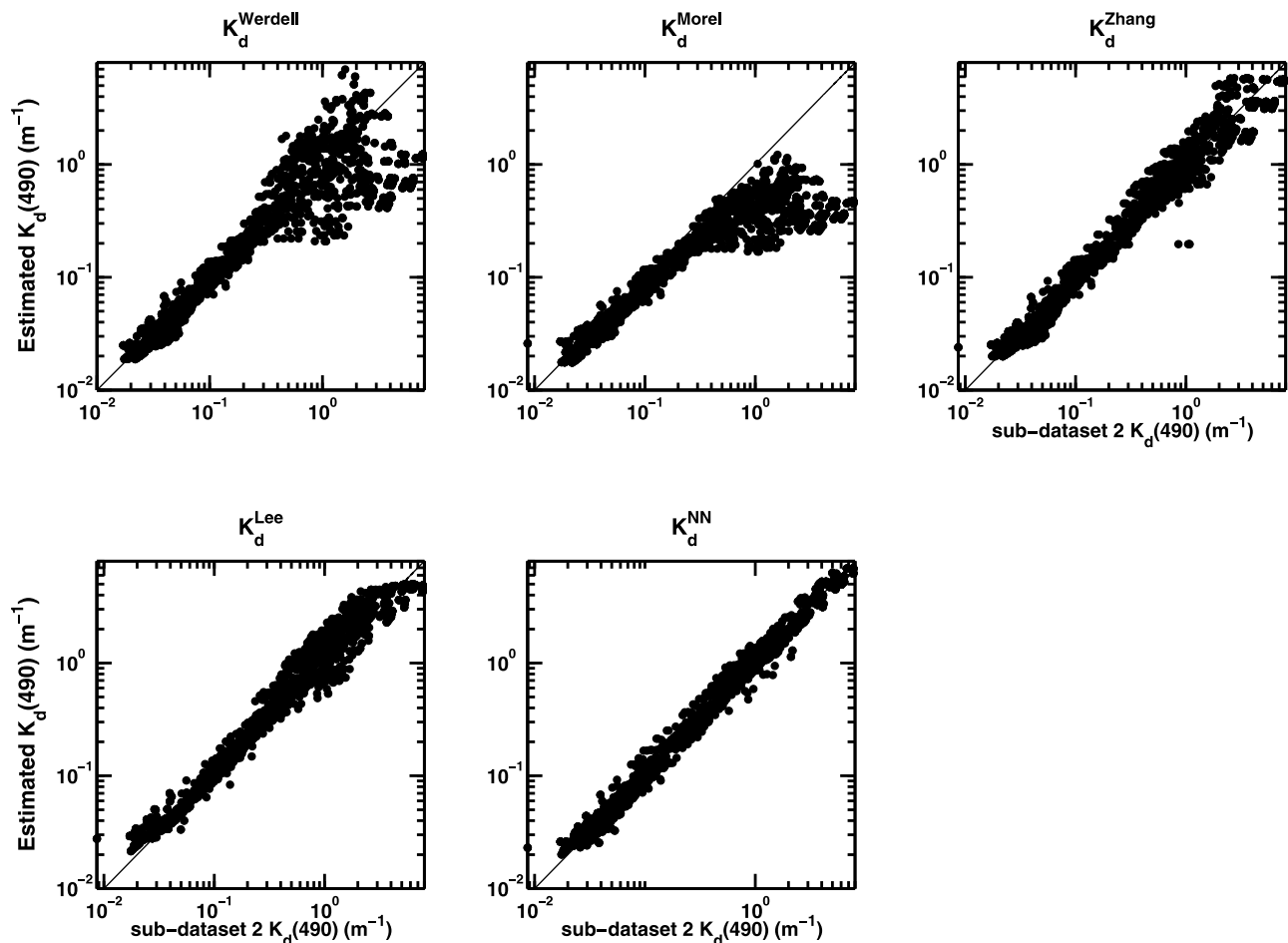


Figure 2. Scatterplots of the desired $K_d(490)$ versus estimated $K_d(490)$ values retrieved with the five algorithms for sub–data set 2. The continuous line represents the 1:1 line.

adapted to MLP, the back-propagation gradient [Bishop, 1995]. The weight values were randomly initialized and the activation function used is the classic sigmoid function with values varying between -1 and 1 . Once the training phase is finished, the MLP will only do algebraic operations, which leads to faster computations, which is very convenient for satellite applications.

[26] As we want to estimate K_d at any wavelength, the sixth visible SeaWiFS R_{rs} between 412 and 670 nm as well as the wavelength at which the K_d retrieval is performed were used as input parameters (Figure 1). Several tests were performed for finding the optimal architecture. Two types of architecture were tested: one or two hidden layers with the number of neurons varying between 1 and 50 for the case with only one hidden layer and between 1 and 20 for the second case (with the number of neurons always higher in the first hidden layer than in the second one). We chose the architecture that combined a minimal error with a minimal number of neurons. Finally, the optimal architecture was therefore composed of one hidden layer MLP with 11 neurons in the hidden layer (Figure 1). Different partitions of the training data set have been tested with no significant differences in the performances of the retrievals. Both the inputs ($R_{rs}(\lambda)$) and output ($\log(K_d(\lambda))$)

of the NN inversion were pre-processed using the following equations:

$$R_{rs}^N(\lambda) = \frac{2}{3} \times \frac{R_{rs}(\lambda) - \text{mean}(R_{rs}(\lambda))}{\sigma(R_{rs}(\lambda))} \quad (10)$$

$$K_d^N(\lambda) = \frac{2}{3} \times \frac{\log(K_d(\lambda)) - \text{mean}(\log(K_d(\lambda)))}{\sigma(\log(K_d(\lambda)))} \quad (11)$$

with σ , the standard deviation. Of course, the output of the NN need to be denormalized with its mean and standard deviation using the invert formulations of equations (10) and (11).

5. Results and Discussion

[27] To demonstrate the performance of the new parametric neural network based inversion, we present inter-comparison results with the existing methods presented in section 2 for $K_d(490)$ and $K_d(\lambda)$ using the sub–data set 2 and the COASTLOOC database. In the following, the discussion of the results will be focused on the retrieval of $K_d(490)$ as all algorithms described in section 2 provide this parameter which is the official parameter provided by NASA. Short discussions about the other SeaWiFS wavelengths will also be provided.

Table 3. Statistical Results for the Retrieval of $K_d(490)$ by the Algorithms of $K_d^{Werdell}$, K_d^{Morel} , K_d^{Zhang} , K_d^{Lee} and K_d^{NN} Applied to the Sub-data Set 2^a

	$K_d^{Werdell}$	K_d^{Zhang}	K_d^{Morel}	K_d^{Lee}	K_d^{NN}
RMSE (m^{-1})	1.41	0.71	1.56	0.53	0.27
RE (%)	29	20	32	20	14
ADP	0.76	0.33	1.31	0.29	0.21
AB (m^{-1})	-0.40	-0.65	-0.08	0.006	-0.011
Slope	0.98	1.05	4.23	1.06	1.03
Intercept	0.41	0.037	0.056	-0.054	-0.014
r	0.47	0.89	0.60	0.94	0.98
# (%) $\in [0.75;1.25]$	64	71	58	73	90

^a# corresponds to the number of points.

[28] The statistical parameters used to assess the performance of the different algorithms are:

[29] 1. The Root-Mean-Square-Error (RMSE):

$$RMSE = \sqrt{\frac{\sum (K_d^{des} - K_d^{est})^2}{N}} \quad (12)$$

with K_d^{est} is the K_d estimated with the different algorithms, K_d^{des} is the desired (measured) K_d and N , the number of examples.

[30] 2. The Relative Error (RE):

$$RE = \frac{1}{N} \times \sum \left(\left| \frac{K_d^{des} - K_d^{est}}{K_d^{des}} \right| \right) \quad (13)$$

[31] 3. The Absolute Difference Percentage (ADP) as defined by Lee et al. [2005a]:

$$ADP = \exp \left(\text{mean} \left| \ln \left(\frac{K_d^{est}}{K_d^{des}} \right) \right| \right) - 1 \quad (14)$$

[32] 4. The average bias (AB):

$$AB = \frac{1}{N} \times \sum (K_d^{est} - K_d^{des}) \quad (15)$$

[33] 5. The slope and intercept of the regression line

[34] 6. The Pearson's correlation coefficient r

5.1. Results on the Sub-data Set 2 for $K_d(490)$

[35] Figure 2 shows the comparison between the desired $K_d(490)$ values and the $K_d(490)$ retrieved values applying the four published algorithms ($K_d^{Werdell}(490)$, $K_d^{Zhang}(490)$, $K_d^{Morel}(490)$, $K_d^{Lee}(490)$) and the neural network approach ($K_d^{NN}(490)$) to the sub-data set 2 (section 3.1). All statistical

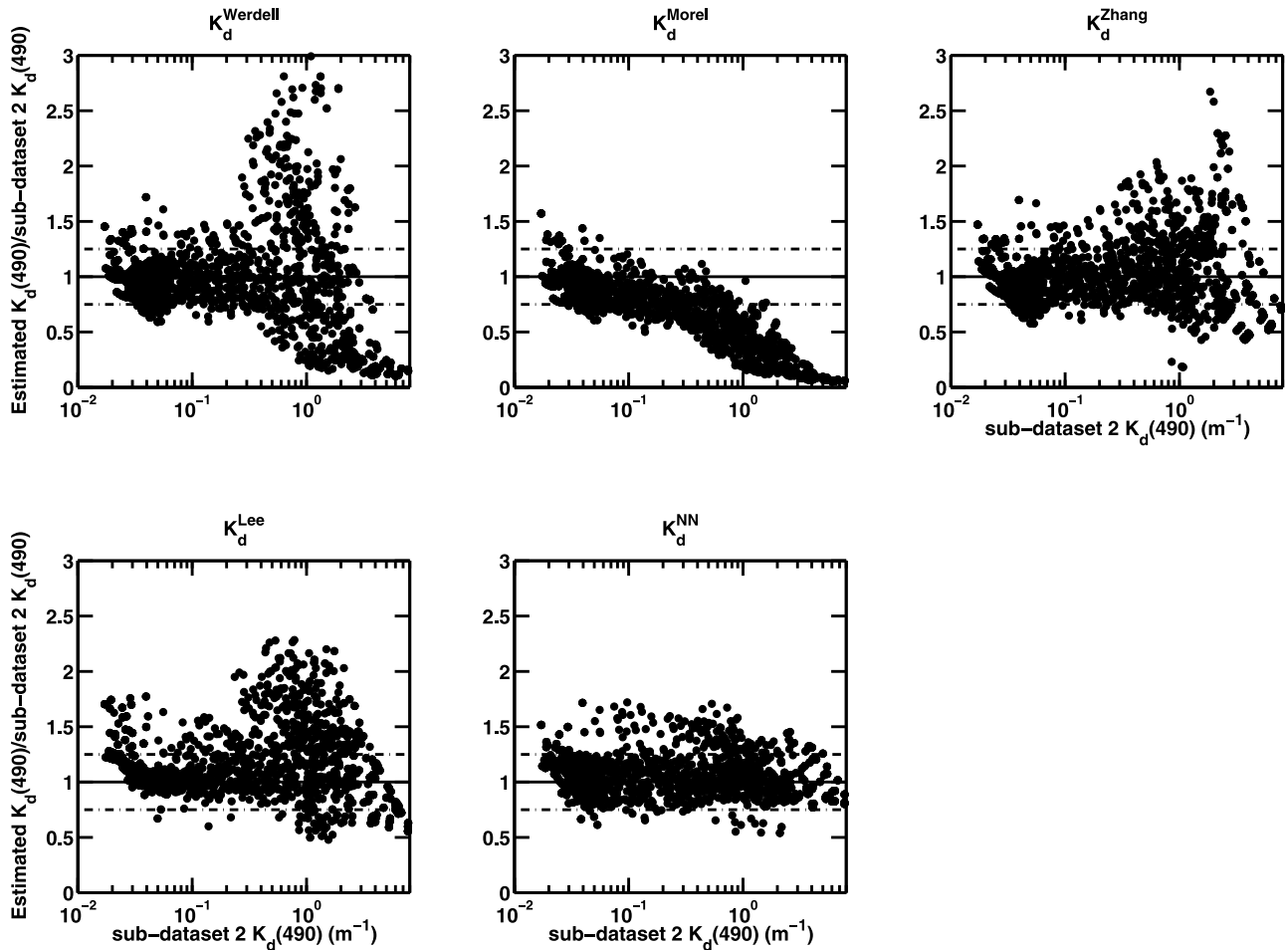


Figure 3. Ratio of the estimated $K_d(490)$ to desired $K_d(490)$ versus desired $K_d(490)$ on the test data set (sub-data set 2) for the five algorithms. The upper vertical dashed line corresponds to a ratio of 1.25, the middle vertical line corresponds to a ratio of 1 and the lower vertical dashed line corresponds to a ratio of 0.75.

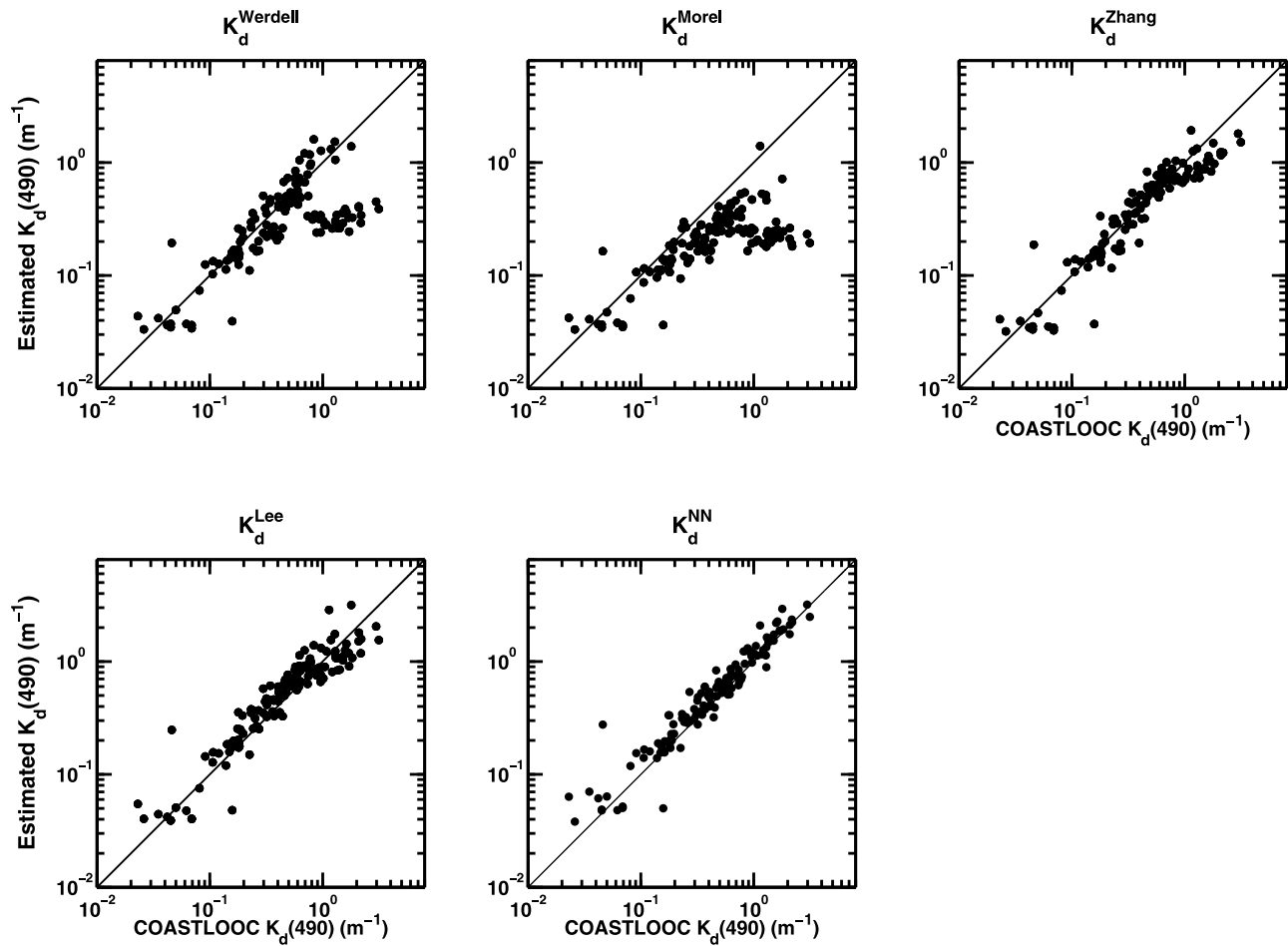


Figure 4. Scatterplots of desired $K_d(490)$ versus estimated $K_d(490)$ values retrieved with the five algorithms for the COASTLOOC data set. From the top left to the bottom right: $K_d^{Werdell}$, K_d^{Morel} , K_d^{Zhang} , K_d^{Lee} and K_d^{NN} . The continuous line represents the 1:1 line.

results are given in Table 3. For the low $K_d(490)$ values, i.e. $<0.25 \text{ m}^{-1}$, all five methods give similar and accurate estimates. The estimates of $K_d(490)$ are very close to the 1:1 line (Figure 2) and the scattering of the data is very low for these low values of $K_d(490)$ (RMSE(K_d^{NN}) = 0.013 m^{-1} , RMSE($K_d^{Werdell}$) = 0.009 m^{-1} , RMSE(K_d^{Morel}) = 0.014 m^{-1} , RMSE(K_d^{Zhang}) = 0.009 m^{-1} , RMSE(K_d^{Lee}) = 0.014 m^{-1}). As shown in Figure 3, most of the retrievals, for any algorithm, have an error within $\pm 25\%$. K_d^{Zhang} , K_d^{Lee} and K_d^{NN} tend to overestimate the very low values of $K_d(490) \leq 0.03 \text{ m}^{-1}$, which is not the case for $K_d^{Werdell}$ and K_d^{Morel} . For moderate and high values, the five algorithms give different results. $K_d^{Werdell}$ and K_d^{Morel} show limitations when $K_d(490)$ is greater than 0.5 m^{-1} with an overall under-estimation of the diffuse attenuation coefficient. K_d^{Zhang} , K_d^{Lee} and K_d^{NN} do not present such limitations. These three algorithms are quite accurate for retrieving $K_d(490) > 0.5 \text{ m}^{-1}$ as shown in Figure 3. K_d^{Zhang} and K_d^{Lee} show overestimates of $K_d(490)$ for values $>1 \text{ m}^{-1}$, of up to 200% (Figure 3). The quality of retrievals obtained with K_d^{NN} do not vary much with $K_d(490)$ (Figures 2 and 3). Only 10% of retrievals have an error $>25\%$ with this latter algorithm, while the number is 36% for $K_d^{Werdell}$, 29% for K_d^{Zhang} , 42% for K_d^{Morel} and 27% for K_d^{Lee} . This is related to the statistical values presented in Table 3, as the RMSE is

0.27 m^{-1} , RE is 14% and the correlation coefficient is 0.98 for the retrievals obtained with K_d^{NN} . The statistical results are computed for the true (linear) values of $K_d(\lambda)$. As the values of this parameter cover a broad range (from 0.08 m^{-1} to 10 m^{-1} so two orders of magnitude), it is interesting to compute statistics with log-transformed $K_d(\lambda)$ through the ADP parameter. As shown in Table 3, when using ADP, the comparison leads to the same conclusion.

[36] These results are in agreement with the conclusions of Lee *et al.* [2005a] who evaluated K_d^{Lee} and previous versions of $K_d^{Werdell}$ and K_d^{Morel} using data collected in three different regions that cover clear open ocean and coastal waters (Gulf of Mexico, the Arabian Sea and the Baltic Sea). The authors showed that $K_d^{Werdell}$ and K_d^{Morel} provided accurate estimates of $K_d(490)$ for the relatively low values, typical of open ocean waters, and under-estimated the $K_d(490)$ for moderate and high values, concluding that these methods were not suitable for turbid waters. This is not surprising that K_d^{Morel} can not retrieve $K_d(490)$ accurately for those range of values, as it has been built for low values of $K_d(\lambda)$ ($<0.5 \text{ m}^{-1}$) and it uses the OC4V6 bio-optical algorithm, that was developed mainly for open ocean waters, for calculating $K_d(\lambda)$. For this study, we used the *Chla* estimated by OC4V6 and not the in-situ *Chla*. It is not the case for $K_d^{Werdell}$ as this algorithm used

Table 4. Statistical Results for the Retrieval of $K_d(490)$ by the Algorithms of $K_d^{Werdell}$, K_d^{Morel} , K_d^{Zhang} , K_d^{Lee} and K_d^{NN} Applied to the Independent COASTLOOC Data Set^a

	$K_d^{Werdell}$	K_d^{Zhang}	K_d^{Morel}	K_d^{Lee}	K_d^{NN}
RMSE (m^{-1})	0.93	0.33	0.70	0.35	0.21
RE (%)	44	26	49	33	28
ADP	1.25	0.48	2.13	0.51	0.38
AB (m^{-1})	-0.19	-0.10	-0.41	0.009	0.09
Slope	0.14	1.34	1.28	0.93	0.88
Intercept	0.58	-0.08	0.34	0.038	0.005
r	0.19	0.87	0.34	0.81	0.96
# (%) $\in [0.75;1.25]$	41	56	22	48	64

^a# corresponds to the number of points.

the NOMAD data set with values of $K_d(490)$ up to $2.29 m^{-1}$. Our results show an improvement of $K_d(490)$ estimates when using a switching point as shown by *Zhang and Fell* [2007]. The development of the latter algorithm is based on the NOMAD data set, like $K_d^{Werdell}$, but this algorithm is able to retrieve moderate and high values of $K_d(490)$. The RMSE is $0.71 m^{-1}$ and r of 0.89 for K_d^{Zhang} while it is

$1.41 m^{-1}$ and r of 0.47 for $K_d^{Werdell}$ (Table 3). K_d^{Lee} also does not show such limitations for the high values of $K_d(490)$, as previously mentioned in *Lee et al.* [2005a]. However, the accuracy of the retrievals is lower than for K_d^{NN} as the RMSE is $0.53 m^{-1}$ and RE is 20% (Table 1). But those retrievals are a bit less biased as AB is $-0.006 m^{-1}$ for K_d^{Lee} and $-0.011 m^{-1}$ for K_d^{NN} .

5.2. Evaluation on the COASTLOOC Data Set

[37] The previous comparison was made using the sub-data set 2. As said in section 3.1, sub-data set 2 is extracted from four data sets, the rest was used to train the NN inversion. So the data used for the training are very similar than those included in sub-data set 2 while it is not the case for developing the four other algorithms. So we present a second validation with the *in-situ* COASTLOOC data set. Using this data set to intercompare the methods can be considered like a blindfold validation as it was not used for parameterizing any of the algorithms.

5.2.1. Comparison of $K_d(490)$

[38] Figure 4 presents the scatterplots of the $K_d(490)$ estimated by the five algorithms versus the COASTLOOC

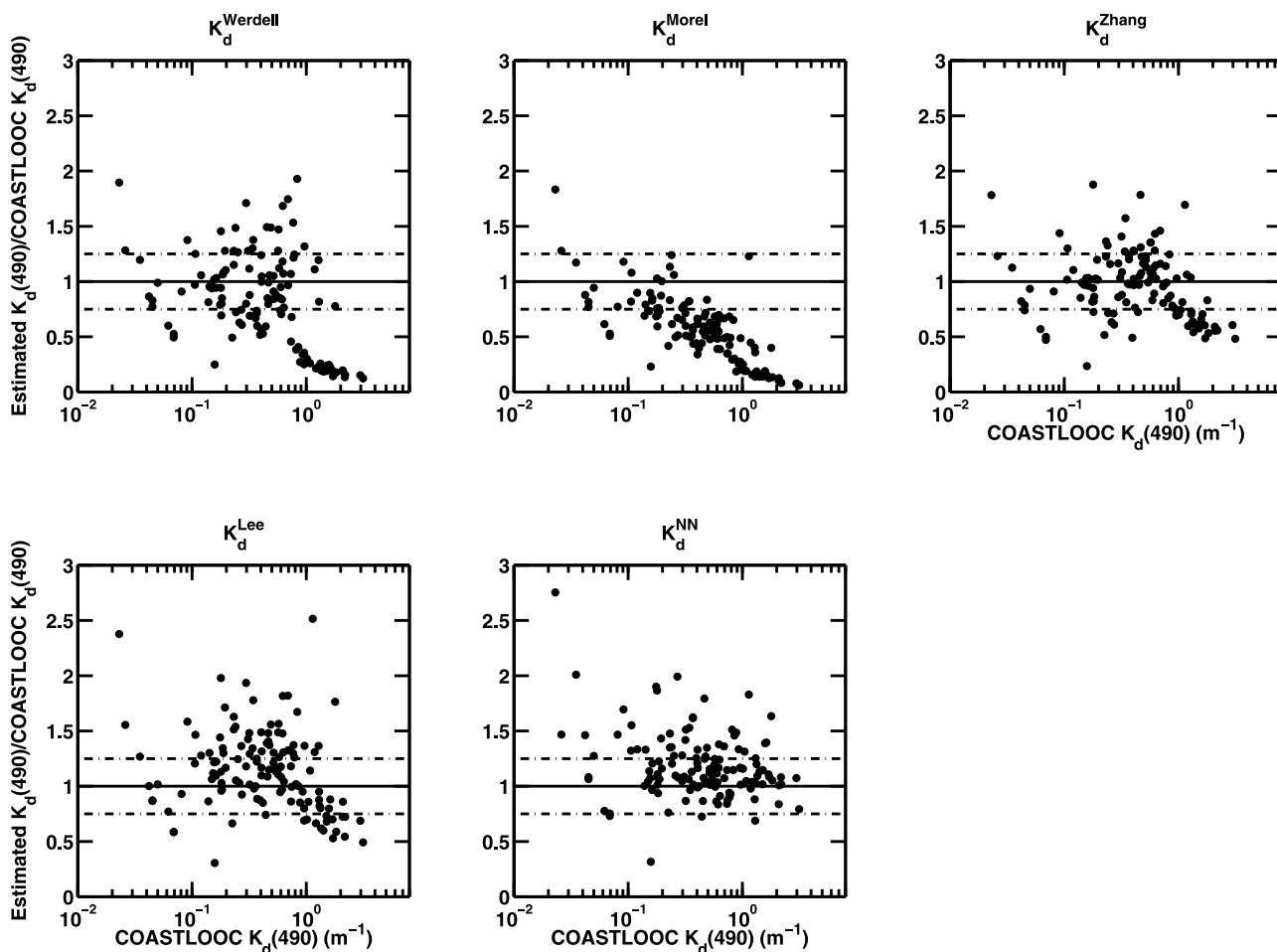


Figure 5. Ratio of the estimated $K_d(490)$ to desired $K_d(490)$ versus desired $K_d(490)$ on the COASTLOOC independent data set for the five algorithms. The upper vertical dashed line corresponds to a ratio of 1.25, the middle vertical line corresponds to a ratio of 1 and the lower vertical dashed line corresponds to a ratio of 0.75.

Table 5. Statistical Results for the Retrieval of $K_d(\lambda)$ by the Algorithms of $K_d^{Werdell}$, K_d^{Morel} , K_d^{Zhang} , K_d^{Lee} and K_d^{NN} Applied to the Independent COASTLOOC Data Set^a

	K_d^{Morel}	K_d^{Lee}	K_d^{NN}
$\lambda = 412 \text{ nm}$			
RMSE (m^{-1})	1.27	0.81	0.61
RE (%)	58	45	33
ADP	3.19	0.68	0.43
AB (m^{-1})	-0.86	0.34	0.28
Slope	1.69	0.65	0.68
Intercept	0.60	0.21	0.19
r	0.40	0.81	0.95
# (%) \in [0.75;1.25]	11	38	59
$\lambda = 443 \text{ nm}$			
RMSE (m^{-1})	0.96	0.62	0.37
RE (%)	50	45	25
ADP	2.35	0.68	0.37
AB (m^{-1})	-0.61	0.24	0.17
Slope	1.39	0.68	0.76
Intercept	0.47	0.14	0.09
r	0.38	0.79	0.96
# (%) \in [0.75;1.25]	18	32	64
$\lambda = 510 \text{ nm}$			
RMSE (m^{-1})	0.64	0.31	0.19
RE (%)	50	37	29
ADP	1.35	0.53	0.39
AB (m^{-1})	-0.13	-0.006	0.03
Slope	0.11	1.02	0.95
Intercept	0.53	-0.005	0.0005
r	0.16	0.83	0.94
# (%) \in [0.75;1.25]	18	53	71
$\lambda = 555 \text{ nm}$			
RMSE (m^{-1})	0.53	0.22	0.19
RE (%)	47	29	25
ADP	2.05	0.45	0.38
AB (m^{-1})	-0.30	-0.014	-0.002
Slope	1.46	1.10	1.03
Intercept	0.23	-0.03	-0.01
r	0.24	0.87	0.90
# (%) \in [0.75;1.25]	24	57	69
$\lambda = 670 \text{ nm}$			
RMSE (m^{-1})	0.47	0.37	0.33
RE (%)	24	34	23
ADP	0.58	0.51	0.33
AB (m^{-1})	-0.25	0.12	0.11
Slope	0.85	0.70	0.63
Intercept	0.34	0.17	0.24
r	0.24	0.59	0.80
# (%) \in [0.75;1.25]	65	48	67

^a# corresponds to the number of points.

$K_d(490)$ measurements. All statistical results are given in Table 4. The comparisons with the COASTLOOC data set lead to the same conclusions than the comparisons with the sub-data set 2.

[39] For the low values of $K_d(490)$, i.e. $<0.25 \text{ m}^{-1}$, all five methods give similar estimates as shown in Figures 4 and 5. Few points are however scattered, especially for the very low values of $K_d(490)$ ($\leq 0.25 \text{ m}^{-1}$). For those low $K_d(490)$ values, the statistical results are relatively similar, as the RMSE is 0.050 m^{-1} for $K_d^{Werdell}$, 0.052 m^{-1} for K_d^{Zhang} , 0.050 m^{-1} for K_d^{Morel} , 0.070 m^{-1} for K_d^{Lee} and 0.068 m^{-1} for K_d^{NN} . The correlation coefficient is almost the same with

values between 0.77 for K_d^{Morel} and 0.80 for K_d^{Lee} . It is worth noting that even if the NN inversion was trained for both open and coastal waters, its retrievals are very comparable with the one obtained with K_d^{Morel} , which was developed only for open ocean waters. The differences in term of RMSE come from the very low values of $K_d(490)$ ($<0.08 \text{ m}^{-1}$) as there were only few training data in this range of $K_d(490)$.

[40] For $K_d(490) > 0.25 \text{ m}^{-1}$, there are, again, differences in the retrieval accuracy depending on the algorithm. As previously shown, $K_d^{Werdell}$ and K_d^{Morel} present limitations when $K_d(490)$ is greater than 0.5 m^{-1} with an overall underestimation of the diffuse attenuation coefficient for both algorithms (Figures 4 and 5), $K_d^{Werdell}$ showing an overestimation for few points (for $K_d(490)$ around 0.8 m^{-1}). As said in the previous section, K_d^{Morel} is developed for case 1 waters and uses the OC4V6 algorithm to calculate $Chla$, which explains its limitation for estimating high values of $K_d(490)$, which is not entirely the case for $K_d^{Werdell}$. Our study shows, again, the same conclusions as in Lee et al. [2005b] with another independent set of data but also as in the work by Zhang and Fell [2007] who evaluated their own parameterization of $K_d(490)$ to $K_d^{Werdell}$ and K_d^{Lee} with the COASTLOOC data set. They showed that using a switching point with $R_{rs}(670)$ instead of $R_{rs}(555)$ allowed a better estimation for high values of $K_d(490)$. This effect can be seen in Figures 4 and 5. From $K_d(490) = 0.7 \text{ m}^{-1}$, $K_d^{Werdell}$ highly underestimates $K_d(490)$ while the values obtained with K_d^{Zhang} are still underestimated but only by 25%, compared to $\approx 75\%$ with $K_d^{Werdell}$.

[41] As said by Lee et al. [2005b], K_d^{Lee} does not have such limitations. All the retrievals are close to the 1:1 line (Figures 4 and 5) and the retrievals are very similar to those of K_d^{Zhang} as the RMSE is 0.40 m^{-1} for K_d^{Zhang} and 0.42 m^{-1} for K_d^{Lee} , for $K_d(490) > 0.25 \text{ m}^{-1}$. The retrievals obtained with the NN inversion show better accuracies for $K_d(490) > 1 \text{ m}^{-1}$ as most of the records have an error $\pm 25\%$ error. It is an improvement of the retrievals compared to K_d^{Zhang} and K_d^{Lee} . For $K_d(490) > 0.25 \text{ m}^{-1}$, the RMSE is 0.25 m^{-1} for K_d^{NN} .

[42] The overall results are given in Table 4. $K_d^{Werdell}$ and K_d^{Morel} are the less accurate methods and show similar accuracies with RMSE of 0.93 m^{-1} and of 0.70 m^{-1} , respectively. K_d^{Zhang} and K_d^{Lee} are quite accurate and also provide similar retrievals, with RMSE of 0.33 m^{-1} and of 0.35 m^{-1} , respectively. This result is in agreement with the study of Zhang and Fell [2007]. K_d^{NN} is the most accurate method to estimate $K_d(490)$ on this independent data set in term of errors (RMSE = 0.21 m^{-1}) as the number of retrievals within $\pm 25\%$ is 64% of the data set, while it is 41% for $K_d^{Werdell}$, 56% for K_d^{Zhang} , 22% for K_d^{Morel} , and 48 for K_d^{Lee} .

5.2.2. Comparison for Other SeaWiFS Wavelengths

[43] As said previously, 490 nm is often the wavelength selected to assess the value of the diffuse attenuation coefficient from remote sensing approaches. Among the different algorithms presented here, the algorithms of Werdell and Zhang and Fell [2007] do not propose any direct estimates of $K_d(\lambda)$, for $\lambda \neq 490 \text{ nm}$. Note that $K_d(\lambda)$ at other wavelengths can be estimated from $K_d(490)$ through empirical relationships [Austin and Petzold, 1986; Kishino et al., 1996]. However, Loisel et al. [2001] showed that these relationships are not universal for wavelengths other than 490 nm. So these two methods have been discarded. K_d^{Morel} ,

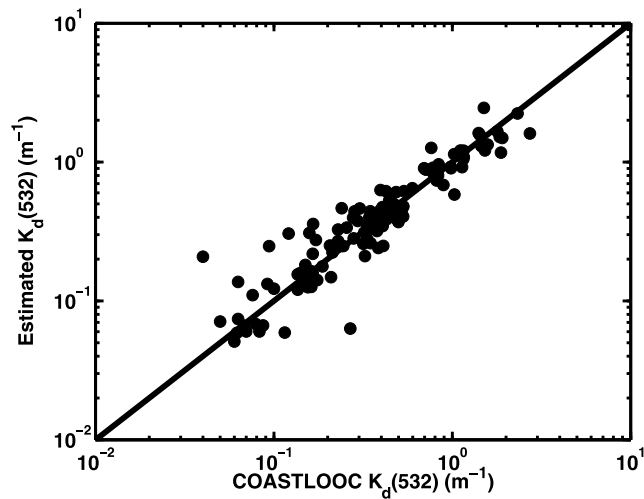


Figure 6. Scatterplot of the desired $K_d(532)$ versus NN-estimated $K_d(532)$ values on the COASTLOOC database.

K_d^{Lee} and K_d^{NN} are compared for the other SeaWiFS wavelengths, i.e. $\lambda = 412, 443, 510, 555$ and 670 nm.

[44] The comparison at the other SeaWiFS wavelengths (Table 5) leads to the same conclusions and results as for $\lambda = 490$ nm. The neural network inversion provides the most accurate values of $K_d(\lambda)$ for any SeaWiFS wavelength in term of RMSE, RE, ADP and r . The correlation coefficient varies between 0.80 ($\lambda = 670$ nm) and 0.96 ($\lambda = 443$ nm). The RMSE varies between 0.19 m^{-1} ($\lambda = 555$ nm) and 0.61 m^{-1} ($\lambda = 412$ nm) and RE between 25% ($\lambda = 443, 555$ nm) and 33% ($\lambda = 510$ nm). The retrievals are somewhat similar between K_d^{Lee} and K_d^{NN} at 555 (RMSE(K_d^{Lee}) = 0.22 m^{-1} ; RMSE(K_d^{NN}) = 0.19 m^{-1}) and 670 nm (RMSE(K_d^{Lee}) = 0.37 m^{-1} ; RMSE(K_d^{NN}) = 0.33 m^{-1}) but they are twice more accurate for the other wavelengths with the NN inversion, in term of RMSE, RE, AD and r . As expected as this model is not suitable for coastal waters, the retrieval obtained with K_d^{Morel} are less accurate with values of RMSE varying between 0.47 m^{-1} at 670 nm and 1.27 m^{-1} at 412 nm.

[45] If the scattering of the data around the 1:1 line is investigated (not shown), the results of K_d^{NN} are less scattered than for the two other methods. This is related to the number of data with an error within $\pm 25\%$. This number varies between 59% and 71% for K_d^{NN} while it is lower for K_d^{Morel} (between 11% and 65%) and K_d^{Lee} (between 32% and 57%) (Table 5). It is worth noting that the quality of the retrievals with K_d^{NN} varies slightly regardless the wavelength.

5.3. Estimation of $K_d(\lambda)$ for a MODIS-AQUA Wavelength

[46] In the previous sections, we showed the efficiency and accuracy of the new neural network inversion, K_d^{NN} , for retrieving $K_d(\lambda)$ at the SeaWiFS wavelengths. Investigations were made to estimate the flexibility of the neural network inversion to estimate K_d at any given wavelength in the visible spectrum using the COASTLOOC data set. Figure 6 shows the results for a MODIS-AQUA wavelength, i.e. for $\lambda = 532$ nm. This band was not taken into account in the training phase to calibrate the neural network inversion

and $R_{rs}(532)$ is not an input parameter of the NN. So this can be seen as a truly blindfold validation of the ability of the NN inversion to estimate K_d at any wavelength. As shown in Figure 6, the NN inversion is able to estimate $K_d(532)$ as most of the data are along the 1:1 line, with a slope coefficient of 1.01 and an intercept of -0.008 . The estimates are more scattered around the 1:1 line than for the SeaWiFS wavelengths, especially for low values of $K_d(532)$ ($< 0.1 \text{ m}^{-1}$), but there is no obvious bias. The retrieval accuracy results confirm the observations of the scatterplot as the RMSE and relative error are 0.19 m^{-1} and 31% , respectively. 71% of the retrievals show a relative error lower within 25% . These results are consistent with the statistical results observed for the SeaWiFS wavelengths (Table 3, 4, and 5).

[47] A second test was made for $\lambda = 456$ nm and the results are very consistent with a RMSE = 0.307 m^{-1} , RE = 26% , $r = 0.97$ and 62% of the retrievals with an error of $\pm 25\%$. This exercise shows ability of the NN inversion to estimate K_d at any wavelength from the SeaWiFS R_{rs} .

5.4. Sensitivity to the Solar Zenith Angle

[48] As mentioned in the introduction, $K_d(\lambda)$ is dependent on the illumination conditions at the sea surface [Kirk, 1984, 1991; Morel and Loisel, 1998], which are mainly driven by the solar zenith angle, θ_s . However, this parameter is not explicitly taken into account in the neural network approach as it is not an input parameter. The reason of this choice is to have an easy method for the end-user without needing to calculate θ_s from the ocean color satellite images, but also to be able to calculate K_d from the Level-3 R_{rs} products over the global ocean (such as weekly or monthly products). As this parameter can influence the diffuse attenuation coefficient, it is necessary to investigate if the K_d^{NN} retrieval accuracy is θ_s -dependent. The sensitivity of the estimates of the NN to θ_s has been investigated using the sub-data set 2. In this latter data set, θ_s varies between 0° and 76° (mean values of 29.59° and standard deviation of 23.89°), with most of the values at $0^\circ, 30^\circ$ or 60° . No trend appears (Figure 7) and the RMSE varies randomly regardless the values of θ_s , i.e. no increase/decrease of the RMSE with increase/decrease of the RMSE. As the NN inversion was trained with a broad range of θ_s , this latter parameter does not seem to influence the accuracy of the estimates and is taken implicitly in the training of the NN inversion.

5.5. Application to the SeaWiFS Images

[49] As an example, one SeaWiFS image was processed using $K_d^{Werdell}$ and K_d^{NN} , in the English Channel/North Sea which are considered as mainly turbid waters [Brylinski et al., 1996; Vantrepotte et al., 2006; Loisel et al., 2007]. The SeaWiFS “true” color image is given in Figure 8. The purpose of processing one SeaWiFS image is to analyze the behavior of the NN inversion, which was trained using simulated and in-situ data sets and to observe any issues (like noise for instance) with the method. Moreover, the NN image is compared to the NASA L2 official $K_d(490)$ product (i.e., $K_d^{Werdell}$). This allows to understand the limit of each algorithm and to compare the dynamic range of $K_d(490)$.

[50] Figure 9 presents the daily map of the $K_d(490)$ obtained with $K_d^{Werdell}$ and the neural network inversion, K_d^{NN} . As expected, K_d^{NN} provides higher values of $K_d(490)$ in

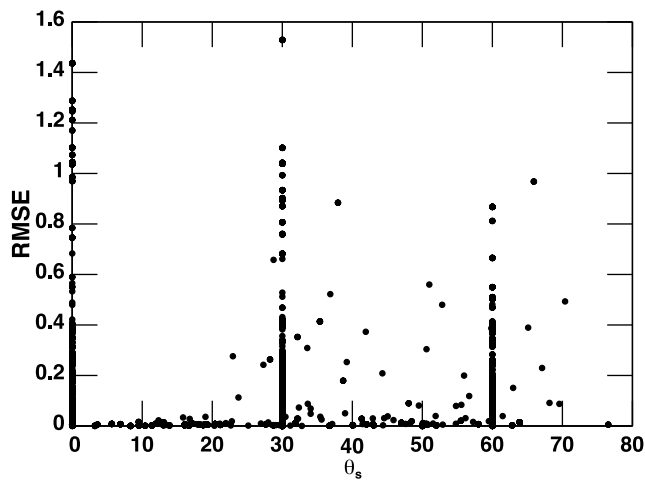


Figure 7. Variation of the RMSE as a function of the solar zenith angle (θ_s) using the training data set (sub-data set 2).

the eastern English Channel and North Sea (Figure 9). The map of $K_d^{Werdell}$ is more homogeneous and shows less contrast between the different seawater masses. The two maps are very different, especially in the eastern English Channel and the North Sea, with differences greater than 150% (Figure 9c). The map obtained with K_d^{NN} shows more patterns with a band of high values of $K_d(490)$ (1.5 m^{-1}), coming from the mouth of the Thames river on the east coast of England. This variation of $K_d(490)$ can be seen in the “true” color image, which allows the comparison of the patterns as a quality control (Figure 8). The patterns observed in the map of K_d^{NN} are very similar to those observed in the “true” color image. The retrieval values of $K_d(490)$ by the two algorithms are very similar in the western English Channel with low values and a slight difference ($\approx 10\%$), where values of $K_d(490)$ are around 0.10 m^{-1} .

[51] K_d^{NN} seems to be more sensitive to clouds and to edges of clouds, as can be seen in the north part of the North Sea. This could be explained by two main factors. First, $K_d^{Werdell}$ uses the ratio of two remote-sensing reflectances. As shown by *Jamet et al.* [2011], the use of ratios of R_{rs} tends to lessen the impact of errors in individual channels. Second, the NN inversion uses the SeaWiFS entire visible spectrum of R_{rs} . If one of the satellite R_{rs} is not correct, it will impact the retrieval of NN inversion. This problem can be difficult to detect prior to the processing.

6. Conclusion

[52] A neural network algorithm has been developed to assess the vertical diffused attenuation of light and validated against in-situ data set (COASTLOOC). The proposed $K_d(\lambda)$ neural network inversion is compared to previous empirical (Werdell [*Morel and Maritorena*, 2001; *Zhang and Fell*, 2007]) and semi-analytical [*Lee et al.*, 2005b] algorithms developed for the SeaWiFS sensor. On the independent COASTLOOC in-situ data set, the retrieval accuracy of the present algorithm is quite similar to published algorithms for oligotrophic and mesotrophic open ocean waters, i.e. for $K_d(490) \leq 0.25 \text{ m}^{-1}$, with RMSE of 0.068 m^{-1} , compared to

0.050 m^{-1} for Werdell, 0.052 m^{-1} for *Zhang and Fell* [2007], 0.050 m^{-1} for *Morel and Maritorena* [2001] and 0.070 m^{-1} for *Lee et al.* [2005b]. For $K_d(490) > 0.25 \text{ m}^{-1}$, the neural network approach allows to retrieve $K_d(490)$ with a much better accuracy than the four other methods as the RMSE is 0.25 m^{-1} with the NN inversion while it is 1.11 m^{-1} for Werdell’s algorithm, 0.40 m^{-1} for *Zhang and Fell* [2007], 0.83 m^{-1} for *Morel and Maritorena* [2001] and 0.42 m^{-1} for *Lee et al.* [2005b]. The results are consistent when comparing for other SeaWiFS wavelengths. One SeaWiFS image is processed in the English Channel/North Sea showing no noise or issues and a broader dynamic of values than the NASA official product, with higher values of $K_d(490)$ in the mouth of Thames river when processed with the NN inversion.

[53] The NN inversion, presented in this study, is able to provide K_d at any visible wavelengths if all remote-sensing reflectances at the SeaWiFS wavelengths are used as input parameters. The NN training should be re-done if one of the SeaWiFS bands is not available (like for MODIS-AQUA). However, if the wavelengths are close enough to the SeaWiFS wavelengths, as, for instance, for the MERIS ocean color sensor, the performance of the present NN approach is conserved (not shown).

[54] The neural network code (in matlab and C) for any ocean color sensor is provided as auxiliary material of this paper and is freely available on-demand by sending an email to cedric.jamet@univ-littoral.fr and it will be implemented

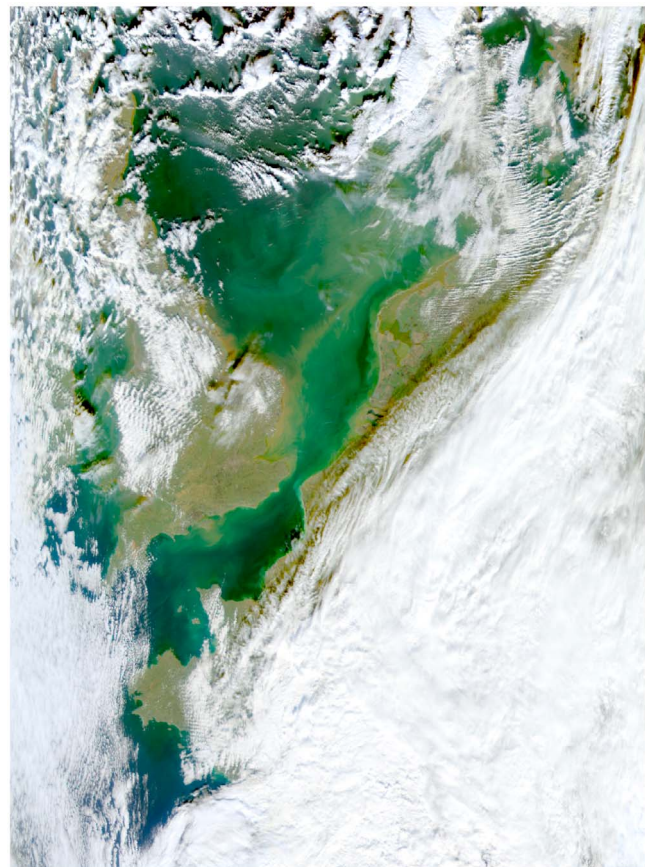


Figure 8. SeaWiFS true color maps over the Eastern English Channel the 31st of March, 2000.

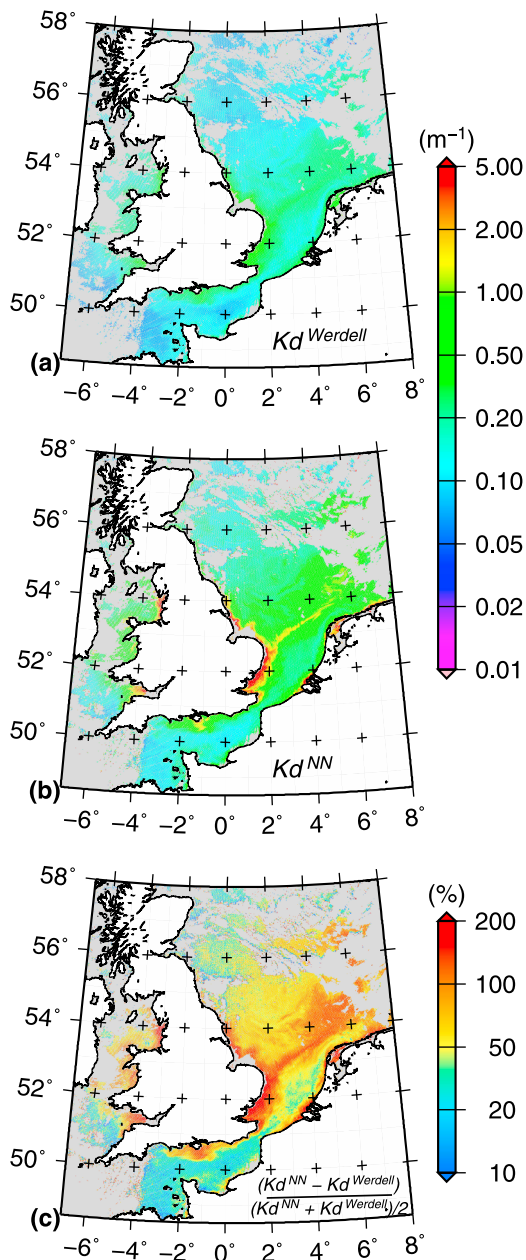


Figure 9. Maps of (a) $K_d^{Werdell}(490)$, (b) $K_d^{NN}(490)$, and (c) the difference between the two methods, over the Eastern English Channel the 31st of March, 2000 for the SeaWiFS sensor.

in the SeaDAS and ODESA software codes.¹ A specific algorithm for MODIS-AQUA will be provided when the training will be finished. The present algorithm can be applied to MERIS data with careful attention to the slight difference between the SeaWiFS and MERIS wavelengths.

Appendix A: Synthetic-Turbid Waters Data Sets

[55] New numerical simulations were carried out for a homogeneous and infinitely deep ocean. The air-sea interface

¹Auxiliary materials are available with the HTML. doi:10.1029/2012JC008076.

was modeled following *Cox and Munk* [1954] with a fixed wind speed of 5 m.s^{-1} . A standard clear atmosphere (with a visibility of 15 km) with three sun zenith angle values (0° , 30° and 60°) was adopted. Raman scattering was omitted as only turbid waters were considered, but *Chla* fluorescence was taken into account in the simulations. Total absorption and attenuation coefficients were fixed as follows:

$$a(\lambda) = a_w(\lambda) + a_{cdom}(\lambda) + a_{phy}(\lambda) + a_{nap}(\lambda) \quad (\text{A1})$$

$$b(\lambda) = b_w(\lambda) + b_{phy}(\lambda) + b_{nap}(\lambda) \quad (\text{A2})$$

[56] Pure sea water absorption, $a_w(\lambda)$, and scattering, $b_w(\lambda)$, coefficients were taken from *Pope and Fry* [1997] and *Smith and Baker*, 1981, respectively. Absorption by colored dissolved organic matter, $a_{cdom}(\lambda)$ was computed as a function of $a_{cdom}(443)$ with an exponential spectral slope value of -0.0176 nm^{-1} [*Babin et al.*, 2003b]. Phytoplankton, $a_{phy}(\lambda)$, and non-algal absorption, $a_{nap}(\lambda)$, coefficients were calculated as a function of the chlorophyll concentration, *Chla*, and suspended particulate matter, *SPM*, using *Bricaud et al.* [1998] and [*Babin et al.* [2003a], respectively. Scattering coefficient by phytoplankton at 660 nm, $b_{phy}(660)$, was calculated as the difference between the attenuation coefficient by phytoplankton, $c_{phy}(660)$, provided by *Loisel and Morel* [1998], and $a_{phy}(660)$. The spectral slope of the attenuation coefficient by phytoplankton was close to zero (0.05), as only high *Chla* concentrations were considered:

$$b_{phy}(\lambda) = \left[0.407(\text{chl } a)^{0.795} \right] \times \left[(\lambda/660)^{-0.05} \right] - a_{phy}(\lambda) \quad (\text{A3})$$

[57] The scattering coefficient by non algal particles was calculated as the difference between the attenuation coefficient by non algal particles and $a_{nap}(\lambda)$ as follows:

$$b_{nap}(\lambda) = \left[0.71 \times (\text{SPM} + a_{nap}(555)) \times \left[(\lambda/555)^{-0.3749} \right] - a_{nap}(\lambda) \right] \quad (\text{A4})$$

where the spectral slope of the attenuation coefficient by non algal particles was set to -0.375 m^{-1} [*Babin et al.*, 2003b], and their specific attenuation coefficient was fixed as in [*Neukermans et al.*, 2012].

[58] The particle phase function for non algal particles was derived from the formulation proposed by *Mobley et al.* [1993], while the formulation of *Fournier and Forand* [1994] with a particulate backscattering to scattering ratio of 0.006 was used for phytoplankton. The simulations were performed for *Chla*, *SPM*, and $a_{cdom}(443)$ values in the following ranges: $[2-70] \text{ mg.m}^{-3}$, $[0.1-120] \text{ g.m}^{-3}$, and $[0.01-5] \text{ m}^{-1}$.

[59] Note that only *Chla*, *SPM*, and $a_{cdom}(443)$ combinations representative of in-situ observations performed in very contrasted bio-optical environments were taken into account [*Babin et al.*, 2003a, 2003b]. For a given parameter, the two others vary in a realistic way according to numerous in situ measurements performed in coastal environments [*Babin et al.*, 2003a; *Loisel et al.*, 2010]. Based on these in situ measurements, when one component was high the two others were relatively high, but the proportions of the three components vary over more than one order of magnitude, which

was taken into account in our simulations. This was a very important result of the paper of *Babin et al.* [2003a]. For instance, for a chlorophyll concentration of 1 (70) $\text{mg}\cdot\text{m}^{-3}$, SPM was allowed to vary between 0.1 (5) and 1 (120) $\text{g}\cdot\text{m}^{-3}$. This was in good agreement with in situ measurements collected in various coastal environments (even if one may observe relatively low chlorophyll concentration in waters with relatively high SPM concentration during resuspension effects for example.)

[60] **Acknowledgments.** The authors would like to thank INSU/CNRS for funding through the PNTS program. The authors acknowledge Marcel Babin for providing the COASTLOOC database, NASA for the NOMAD database and the SeaWiFS images and the IOCCG for the synthetic database.

References

- Atkinson, P. M., and A. R. L. Tatnall (1997), Neural networks in remote sensing: Introduction, *Int. J. Remote Sens.*, *18*, 699–709.
- Austin, R. W., and T. J. Petzold (1981), The determination of the diffuse attenuation coefficient of sea water using the coastal zone color scanner, in *Oceanography From Space*, edited by J. F. R. Gower, pp. 239–256, Springer, New York.
- Austin, R. W., and T. J. Petzold (1986), Spectral dependence of the diffuse attenuation coefficient of light in ocean waters, *Opt. Eng.*, *25*, 471–479.
- Babin, M., D. Stramski, G. M. Ferrari, H. Claustre, A. Bricaud, G. Obolensky, and N. Hoepffner (2003a), Variation in the light absorption coefficient of phytoplankton, nonalgal particles and dissolved organic matter in coastal waters around Europe, *J. Geophys. Res.*, *108*(C7), 3211, doi:10.1029/2001JC000882.
- Babin, M., A. Morel, V. Fournier-Sicre, F. Fell, and D. Stramski (2003b), Light scattering properties of marine particles in coastal and open ocean waters as related to the particle mass concentration, *Limnol. Oceanogr.*, *48*, 843–859, doi:10.4319/lo.2003.48.2.0843.
- Badran, F., and S. Thiria (2002), Multilayered perceptron: From the non-linear regression to inverse problems, *J. Phys. IV*, *12*, 1157–1188.
- Bishop, C. M. (1995), *Neural Networks for Pattern Recognition*, 482 pp., Oxford Univ. Press, Oxford, U. K.
- Brajard, J., C. Jamet, C. Moulin, and S. Thiria (2006a), Use of a neuro-variational inversion for retrieving oceanic and atmospheric constituents from satellite ocean colour sensor: Application to absorbing aerosols, *Neural Networks*, *19*, 178–185.
- Brajard, J., C. Jamet, C. Moulin, and S. Thiria (2006b), Validation of a neuro-variational inversion of ocean colour images, *Adv. Space Res.*, *38*, 2169–2175.
- Brajard, J., C. Moulin, and S. Thiria (2008), Atmospheric correction of SeaWiFS ocean color imagery in the presence of absorbing aerosols off the Indian coast using a neuro-variational method, *Geophys. Res. Lett.*, *35*, L20604, doi:10.1029/2008GL035179.
- Bricaud, A., A. Morel, M. Babin, K. Allali, and H. Claustre (1998), Variations of light absorption by suspended particles with chlorophyll a concentration in oceanic (case 1) waters: Analysis and implications for bio-optical models, *J. Geophys. Res.*, *103*, 31,033–31,044.
- Bricaud, A., C. Mejjia, D. Biondeau-Patissier, H. Claustre, M. Crepon, and S. Thiria (2007), Retrieval of pigment concentrations and size structure of algal populations from their absorption spectra using multilayered perceptrons, *Appl. Opt.*, *46*, 1251–1260.
- Brylinski, J. M., C. Brunet, D. Bentley, G. Thoumelin, and D. Hilde (1996), Hydrography and phytoplankton biomass in eastern English Channel in spring 1992, *Estuarine Coastal Shelf Sci.*, *43*, 507–519.
- Buckton, D., E. O'Mongain, and S. Danaher (1999), The use of neural networks for the estimation of oceanic constituents based on the MERIS instrument, *Int. J. Remote Sens.*, *20*, 1841–1851.
- Cox, C., and W. Munk (1954), Measurement of the roughness of the sea surface from photographs of the Sun's glitter, *J. Opt. Soc. Am.*, *44*, 838–850.
- Cybenko, G. (1989), Approximation by superposition of a sigmoidal function, *Math. Control. Signal Syst.*, *2*, 303–313.
- D'Alimonte, D., and G. Zibordi (2003), Phytoplankton determination in an optically complex coastal region using a multilayer perceptron neural network, *IEEE Trans. Geosci. Remote Sens.*, *41*, 2861–2868.
- Doerffer, R., and H. Schiller (2007), The MERIS case 2 water algorithm, *Int. J. Remote Sens.*, *28*, 517–535.
- Doron, M., M. Babin, A. Mangin, and O. Hembise (2007), Estimation of light penetration, and horizontal and vertical visibility in oceanic and coastal waters from surface reflectance, *J. Geophys. Res.*, *112*, C06003, doi:10.1029/2006JC004007.
- Fournier, G., and J. L. Forand (1994), Analytic phase function for ocean water, in *Ocean Optics XII*, edited by J. S. Jaffe, *Proc. SPIE*, *2258*, 194–201.
- Gardner, M. W., and S. R. Dorling (1998), Artificial neural networks (the multilayer perceptron): A review of applications in the atmospheric sciences, *Atmos. Environ.*, *32*, 2627–2636.
- Gonzales Vilas, L., E. Spyarakos, and J. M. Torres-Palenzuela (2011), Neural network estimation of chlorophyll a from MERIS full resolution data for the coastal waters of Galician rias (NW Spain), *Remote Sens. Environ.*, *115*, 524–535.
- Gordon, H. R. (1989), Can the Lambert-Beer law be applied to the diffuse attenuation coefficient of ocean water, *Limnol. Oceanogr.*, *34*, 1389–1409.
- Gross, L., S. Thiria, R. Frouin, and B. G. Mitchell (2000), Artificial neural network for modeling the transfer function between marine reflectance and phytoplankton pigment concentration, *J. Geophys. Res.*, *105*, 3483–3495.
- Hornik, K., M. Stinchcomb, and F. E. Muller-Krager (1989), Multilayer feedforward networks are universal approximators, *Neural Networks*, *2*, 359–366.
- Ioannou, I., A. Gilerson, B. Gross, F. Moshary, and S. Ahmed (2011), Neural network approach to retrieve the inherent optical properties of the ocean from observations of MODIS, *Appl. Opt.*, *50*, 3168–3186.
- IOCCG (2006), Remote sensing of inherent optical properties: Fundamentals, tests of algorithms, and applications, edited by Z. P. Lee, *IOCCG Rep. 5*, 122 pp., Dartmouth, N. S., Canada.
- Jamet, C., C. Moulin, and S. Thiria (2004), Monitoring aerosol optical properties over the Mediterranean from SeaWiFS images using a neural network inversion, *Geophys. Res. Lett.*, *31*, L13107, doi:10.1029/2004GL019951.
- Jamet, C., S. Thiria, C. Moulin, and M. Crepon (2005), Use of a neuro-variational inversion for retrieving oceanic and atmospheric constituents from ocean color imagery: A feasibility study, *J. Atmos. Ocean. Tech.*, *22*, 460–475.
- Jamet, C., H. Loisel, C. P. Kuchinke, K. Ruddick, G. Zibordi, and H. Feng (2011), Comparison of three SeaWiFS atmospheric correction algorithms for turbid waters using AERONET-OC measurements, *Remote Sens. Environ.*, *115*, 1955–1965.
- Keiner, L. E., and C. W. Brown (1999), Estimating oceanic chlorophyll concentrations with neural networks, *Int. J. Remote Sens.*, *20*, 189–194.
- Kirk, J. T. O. (1984), Dependence of relationship between inherent and apparent optical properties of water on solar altitude, *Limnol. Oceanogr.*, *29*, 350–356.
- Kirk, J. T. O. (1991), Volume scattering function, average cosines, and the underwater light field, *Limnol. Oceanogr.*, *36*, 455–467.
- Kishino, M., J. Ishizaka, H. Satoh, K. Kusaka, S. Saitoh, T. Miyoi, and K. Kawasaki (1996), Optical characteristics of sea water in the north Pacific ocean, in *Ocean Optics XIII*, edited by S. G. Ackleson and R. Frouin, *Proc. SPIE*, *2963*, 173–178.
- Krasnopolsky, V. M. (2007), Neural network emulations for complex multidimensional geophysical mappings: Applications of neural network techniques to atmospheric and oceanic satellite retrievals and numerical modeling, *Rev. Geophys.*, *45*, RG3009, doi:10.1029/2006RG000200.
- Krasnopolsky, V. M., and H. Schiller (2003), Some neural network applications in environmental sciences. Part I: Forward and inverse problems in geophysical remote measurements, *Neural Net.*, *16*, 321–334.
- Kratzer, S., C. Brockmann, and G. Moore (2008), Using MERIS full resolution data to monitor coastal waters: A case study from Himmerfjorden, a fjord-like bay in the northwestern Baltic Sea, *Remote Sens. Environ.*, *112*, 2284–2300.
- Lee, Z. P., K. L. Carder, and R. Arnone (2002), Deriving inherent optical properties from water color: A multi-band quasi-analytical algorithm for optically deep waters, *Appl. Opt.*, *41*, 5755–5772, doi:10.1364/AO.41.005755.
- Lee, Z. P., M. Darecki, K. Carder, C. Davis, D. Stramski, and W. Rhea (2005a), Diffuse attenuation coefficient of downwelling irradiance: An evaluation of remote sensing methods, *J. Geophys. Res.*, *110*, C02017, doi:10.1029/2004JC002573.
- Lee, Z. P., K. Du, and R. Arnone (2005b), A model for the diffuse attenuation coefficient of downwelling irradiance, *J. Geophys. Res.*, *110*, C02016, doi:10.1029/2004JC002275.
- Lee, Z. P., A. Weideman, J. Kindle, R. Arnone, K. Carder, and C. Davis (2007), Euphotic zone depth: its derivation and implication to ocean-color remote sensing, *J. Geophys. Res.*, *112*, C03009, doi:10.1029/2006JC003802.

- Lewis, M., M. Carr, G. Feldman, W. E. Esaias, and C. R. McClain (1990), Influence of the penetrating solar radiation on the heat budget of the equatorial Pacific Ocean, *Nature*, *347*, 543–545, doi:10.1038/347543a0.
- Loisel, H., and A. Morel (1998), Light scattering and chlorophyll concentration in case 1 waters: A re-examination, *Limnol. Oceanogr.*, *43*, 847–857.
- Loisel, H., D. Stramski, B. G. Mitchell, F. Fell, V. Fourniser-Sicre, B. Lemasle, and M. Babin (2001), Comparison of the ocean inherent optical properties obtained from measurements and inverse modeling, *Appl. Opt.*, *40*, 2384–2397.
- Loisel, H., X. Mériaux, J.-F. Berthon, and A. Poteau (2007), Investigation of the optical backscattering ratio of marine particles in relation to their biogeochemical composition in the eastern English Channel and southern North Sea, *Limnol. Oceanogr.*, *52*, 739–752.
- Loisel, H., B. Lubac, D. Dessailly, L. Dufort-Gaurier, and V. Vantrepotte (2010), Effect of inherent optical properties variability on the chlorophyll retrieval from ocean color remote sensing: An in situ approach, *Opt. Express*, *18*, 20,949–20,959.
- Loisel, H., et al. (2011), Characterization of the bio-optical anomaly and diurnal variability of particulate matter, as seen from scattering and backscattering coefficients, in ultra-oligotrophic eddies of the Mediterranean Sea, *Biogeosciences*, *8*, 3295–3317. doi:10.5194/bg-8-3295-2011.
- Mobley, C. D. (1994), *Light and Water: Radiative Transfer in Natural Waters*, 592 pp., Academic, New York.
- Mobley, C. D. (1995), *Hydrolight 3.0 USers' Guide*, SRI Int., Menlo Park, Calif.
- Mobley, C. D., B. Gentili, H. R. Gordon, Z. Jin, G. W. Kattawar, A. Morel, P. Reinersman, K. Stamnes, and R. H. Stavn (1993), Comparison of numerical models for computing underwater light fields, *Appl. Opt.*, *32*, 7484–7504.
- Morel, A. (1988), Optical modeling of the upper ocean in relation to its biogenous matter content (case 1 waters), *J. Geophys. Res.*, *93*, 10,749–10,768.
- Morel, A., and D. Antoine (1994), Heating rate within the upper ocean in relation to its bio-optical state, *J. Phys. Oceanogr.*, *24*, 1652–1665.
- Morel, A., and H. Loisel (1998), Apparent Optical properties of oceanic waters: dependence on molecular scattering contribution, *Appl. Opt.*, *37*, 4765–4776.
- Morel, A., and S. Maritorena (2001), Bio-optical properties of oceanic waters: A reappraisal, *J. Geophys. Res.*, *106*, 7163–7180, doi:10.1029/2000JC000319.
- Morel, A., Y. Huot, B. Gentili, P. J. Werdell, S. B. Hooker, and B. A. Franz (2007), Examining the consistency of products derived from various ocean color sensors in open ocean (case 1) waters in the perspective of a multi-sensor approach, *Remote Sens. Environ.*, *111*, 69–88, doi:10.1016/j.rse.2007.03.012.
- Mueller, J. L. (2000), SeaWiFS algorithm for the diffuse attenuation coefficient, $K(490)$, using water-leaving radiances at 490 and 555 nm, in *SeaWiFS Postlaunch Calibration and Validation Analyses*, part 3, edited by S. B. Hooker, pp. 24–27, NASA Goddard Space Flight Cent., Greenbelt, Md.
- Neukermans, G., H. Loisel, X. Mériaux, R. Astoreca, and D. McKee (2012), In situ variability of mass-specific beam attenuation and backscattering of marine particles with respect to particle size, density, and composition, *Limnol. Oceanogr.*, *57*, 124–144.
- Pinkus, A. (1999), Approximation theory of the MLP model in neural networks, *Acta Numerica*, *8*, 143–195.
- Platt, T., S. Sathyendranath, C. Caverhill, and M. Lewis (1988), Ocean primary production and available light: Further algorithms for remote sensing, *Deep Sea Res. Part I*, *35*, 855–879.
- Pope, R. M., and E. S. Fry (1997), Absorption spectrum (380–700 nm) of pure water. II. Integrating cavity measurements, *Appl. Opt.*, *36*, 8710–8723.
- Preisendorfer, R. W. (1975), *Hydrologic Optics*, vol. 1, *Introduction*, Natl. Tech. Inf. Serv., Springfield, Va.
- Preisendorfer, R. W. (1986), Secchi disk science: Visual optics of natural waters, *Limnol. Oceanogr.*, *31*, 909–926.
- Rumelhart, D. E., G. E. Hinton, and R. J. Williams (1986), Learning internal representations by error propagation, in *Parallel Distributed Processing*, vol. 1, edited by D. E. Rumelhart, J. L. McClelland, and P. R. Group, pp. 318–6362, MIT Press, Cambridge, Mass.
- Sathyendranath, S., A. D. Gouveia, S. Shetye, P. Ravindran, and T. Platt (1989), Biological control of surface temperature in the Arabian Sea, *Nature*, *349*, 54–56.
- Sathyendranath, S., T. Platt, C. Caverhill, R. Warnock, and M. Lewis (1991), Remote sensing of oceanic primary production: Computations using a spectral model, *Deep Sea Res.*, *36*, 431–453.
- Schiller, H., and R. Doerffer (1997), Neural network for the evaluation of the inverse model: Operational derivation of case 2 water properties from MERIS data, *Int. J. Remote Sens.*, *20*, 1735–1746.
- Schroeder, T., I. Behnert, M. Schaale, J. Fischer, and R. Doerffer (2007), Atmospheric correction algorithm for MERIS above case-2 waters, *Int. J. Remote Sens.*, *28*, 1469–1486.
- Smith, R. C., and K. S. Baker (1981), Optical properties of the clearest natural waters (200–800 nm), *Appl. Opt.*, *20*, 177–184.
- Tanaka, A., M. Kishino, R. Doerffer, H. Schiller, T. Oishi, and T. Kubota (2004), Development of a neural network algorithm for retrieving concentrations of chlorophyll, suspended matter and yellow substance from radiance data of the ocean color and temperature scanner, *J. Oceanogr.*, *60*, 519–530.
- Thiria, S., C. Mejia, F. Badran, and M. Crepon (1993), A neural network approach for modelling transfer functions: Applications for wind retrieval from spaceborne scatterometer data, *J. Geophys. Res.*, *98*, 22,827–22,841.
- Tyler, J. E. (1968), Secchi disc, *Limnol. Oceanogr.*, *13*, 1–6.
- Vantrepotte, V., C. Brunet, X. Mériaux, E. Lécuyer, V. Vellucci, and R. Santer (2006), Bio-optical properties of coastal waters in the Eastern English Channel, *Estuarine Coastal Shelf Sci.*, *72*, 202–212. doi:10.1016/j.ecss.2006.10.016.
- Wang, M., S. Son, and L. W. Harding Jr. (2009), Retrieval of diffuse attenuation coefficient in the Chesapeake Bay and turbid ocean regions for satellite ocean color applications, *J. Geophys. Res.*, *114*, C10011, doi:10.1029/2009JC005286.
- Werdell, P. J., and S. W. Bailey (2005), An improved in-situ bio-optical data set for ocean color algorithm development and satellite data product validation, *Remote Sens. Environ.*, *98*, 122–140, doi:10.1016/j.rse.2005.07.001.
- Zhang, T., and F. Fell (2007), An empirical algorithm for determining the diffuse attenuation coefficient K_d in clear and turbid waters from spectral remote sensing reflectance, *Limnol. Oceanogr. Methods*, *5*, 457–462.
- Zhang, T., F. Fell, Z. S. Liu, R. Preusker, J. Fischer, and M. X. He (2003), Evaluating the performance of artificial neural network techniques for pigment retrieval from ocean color in case I waters, *J. Geophys. Res.*, *108*(C9), 3286, doi:10.1029/2002JC001638.